PRE-PRINT ARTICLE

COPYRIGHT BY COMPOSITES THEORY AND PRACTICE JOURNAL

ISSN: 2299-128X

Investigation of GNP effect on Mechanical and Morphological Characteristics of Liquid Phase Sintered SS316L Nanocomposites processed via Mechanical Alloying and Pressureless Sintering

Kalyanamanohar Veeramallu[1*], Alluru.Gopala Krishna[2]

[1,2] *Department Mechanical Engineering, University College of Engineering Kakinada (A), JNTUK Kakinada, 533003, Andhra Pradesh, India.*

[*]*Corresponding author: kalyanamanohar@jntucek.ac.in*

https://doi.org/10.62753/ctp.2024.03.2.2

Abstract

This study focuses on the development of stainless steel (SS) 316L nanocomposites reinforced with graphene nanoplatelets (GNP) employing the pressureless sintering technique. The optimal pressure of 600 MPa was used to obtain green composite samples. Composite samples with GNP weight percentages of 0.25, 0.5, and 0.75 were sintered at 1400°C for 90 minutes under vacuum of 0.001 mbar. The effect of the GNP reinforcement on the SS316L composites was investigated by means of microstructure observations and mechanical tests. The observations of the microstructure of the composite samples revealed equiaxed and twin-grain structures, implying austenite. Grain refinement can be observed as a consequence of the addition of GNP up to 0.5 wt% in the SS316L matrix. GNP were found to be an effective reinforcement in improving the hardness (287.7 Hv) and ultimate tensile strength (554.62 MPa). However, for the 0.75 wt% GNP composite samples, issues like agglomeration, grain coarsening, and the presence of a grain boundary precipitate (Cr_7C_3) resulted in a deterioration of the mechanical properties.

Keywords: SS316L, graphene nanoplatelets, grain boundary precipitate, carbides, tensile strength

1. Introduction

SS316L is a significant functional material used in exhaust manifolds, furnace parts, aerospace, chemical, and food processing industries because of its attractive properties and exceptional corrosion resistance compared to ferritic steels [1,2]. These steels have better resistance to stress corrosion cracking and have become important structural materials in automobile and aerospace applications [3]. On the other hand, stainless steel 316L possesses lower mechanical strength, corrosion and wear resistance due to its high relative density, and intrinsic porosity limits its wider applications. However, the above properties could be improved by altering the process parameters such as the sintering temperature, sintering atmosphere, holding time, and the dispersion of different alloys that promote higher densification behavior.

In general, stainless steels are compacted and pressureless sintering is performed at lower sintering

PRE-PRINT ARTICLE
COPYRIGHT BY COMPOSITES THEORY AND PRACTICE JOURNAL
ISSN: 2299-128X

temperatures. Consequently, intrinsic porosity was observed in the sintered samples, leading to poor densification. Pandya et al. investigated the large, irregular, and localized pores that formed along the grain boundaries at lower sintering temperatures (1200ºC and 1300ºC). The sintered density and mechanical properties of supersolidus sintered samples were better compared to the solid-state sintered samples [4] Panda et al. developed 316L stainless steel and 316L-YAG composites via conventional and microwave sintering processes at the solid-state and supersolidus sintering temperatures of 1200°C and 1400°C. The experimental results revealed better densification, and grain coarsening was restricted for austenitic and ferritic stainless steels at the liquidus temperature of 1400ºC [2].

Numerous micro- and nano-sized compounds have been used as reinforcing materials in austenitic stainless steels [5–7]. Carbon-based nanomaterials are the perfect choice to be introduced as reinforcement because of their remarkable combination of mechanical, electrical, and thermal properties [8,9]. Graphene nanoplatelets (GNP) have been used for many applications including in composites, coatings, energy storage, as well as in electronics, and bio-medical fields owing to their high elastic modulus, thermal conductivity, and strength [10, 11]. In comparison to carbon nanotubes (CNTs), GNP reinforcement effectively bonds with the matrix material, which results in a further increase in strength [12]. The right proportion of nano-reinforcement in austenitic stainless steels is the most challenging task. Ali et al. prepared stainless steel composites with an addition of 0.25 wt% boron at different pressures ranging from 100 MPa to 600 MPa, and the sintering temperature of 1200°C for 1 hour. A notable increment was found in the hardness, densification, and strength of the sintered samples as a consequence of grain size strengthening [13]. Sadooghi et al. added 2 wt% TiC particles and 2 wt% hexagonal boron nitride (hBN) particles to stainless steel 316L to develop composites. The powders were combined for 5 hours in high-energy ball milling and then compressed at pressures of 350 and 450 MPa after being sintered in a furnace for 2 and 4 hours at 1350°C and 1450°C. It was found that adding reinforcing particles like TiC and hBN results in increasing the hardness and coefficient of friction of SS316L MMCs [14]. Sravan Kumar et al. fabricated Y_2O_3/TiO_2 reinforced 304L stainless steel nanocomposites via the mechanical alloying (MA) route. They reported that the hardness grew with the addition of nanoparticle reinforcement in the 304L steel matrix [15]. Zengin et al. developed 316L/CNTs stainless steel nanocomposites by powder metallurgy (PM). They noticed that the hardness of the nanocomposite increased with an increment in CNT incorporation due to better sintering conditions [16]. Radhamani et al. reinforced 316L stainless steel (SS) with CNTs using the spark plasma sintering technique at 800ºC. Microstructural investigations revealed grain refinement owing to the inclusion of CNTs, which improved the hardness and tensile strength [17].

Though several researchers have concentrated on stainless steel composites with different nano-reinforcements and employing different methods, still, there is a need to understand the effect of

PRE-PRINT ARTICLE
COPYRIGHT BY COMPOSITES THEORY AND PRACTICE JOURNAL
ISSN: 2299-128X

carbonaceous materials. Specifically,the effect of graphene nanoplatelet (GNP) reinforcement on the properties of stainless steel 316L composites via pressureless sintering has not been studied to date. Hence, this research work is aimed to investigate the effect of the addition of GNP reinforcement on the properties of the SS316L matrix at different weight percentages - 0.25, 0.5, and 0.75. The composites were fabricated utilizing mechanical alloying followed by pressureless sintering. The developed composites were investigated by means of microstructural examinations and mechanical tests.

2. Materials and methods

2.1 Powder analysis

SS316L powder (diameter <45 μm; Ni 10-14%, Cr 16-18%, Mo 2-3%, C 0.03%, Fe - balance, Innomet Advanced Materials Pvt. Ltd., India) and GNP (thickness =3-5 nm; diameter < 5 μm; United Nanotech Pvt. Ltd, India) were used as the starting materials to produce SS316L-GNP composites. An SEM micrograph and the particle size distribution of the as-received SS316L powder, which is spherical with a mean particle size of 25.18 μm, are shown in Fig. 1(a) and (b). The stack-like morphology of the as-received GNPs and their elemental composition are presented in Fig. 1(c) and (d).

PRE-PRINT ARTICLE
COPYRIGHT BY COMPOSITES THEORY AND PRACTICE JOURNAL
ISSN: 2299-128X

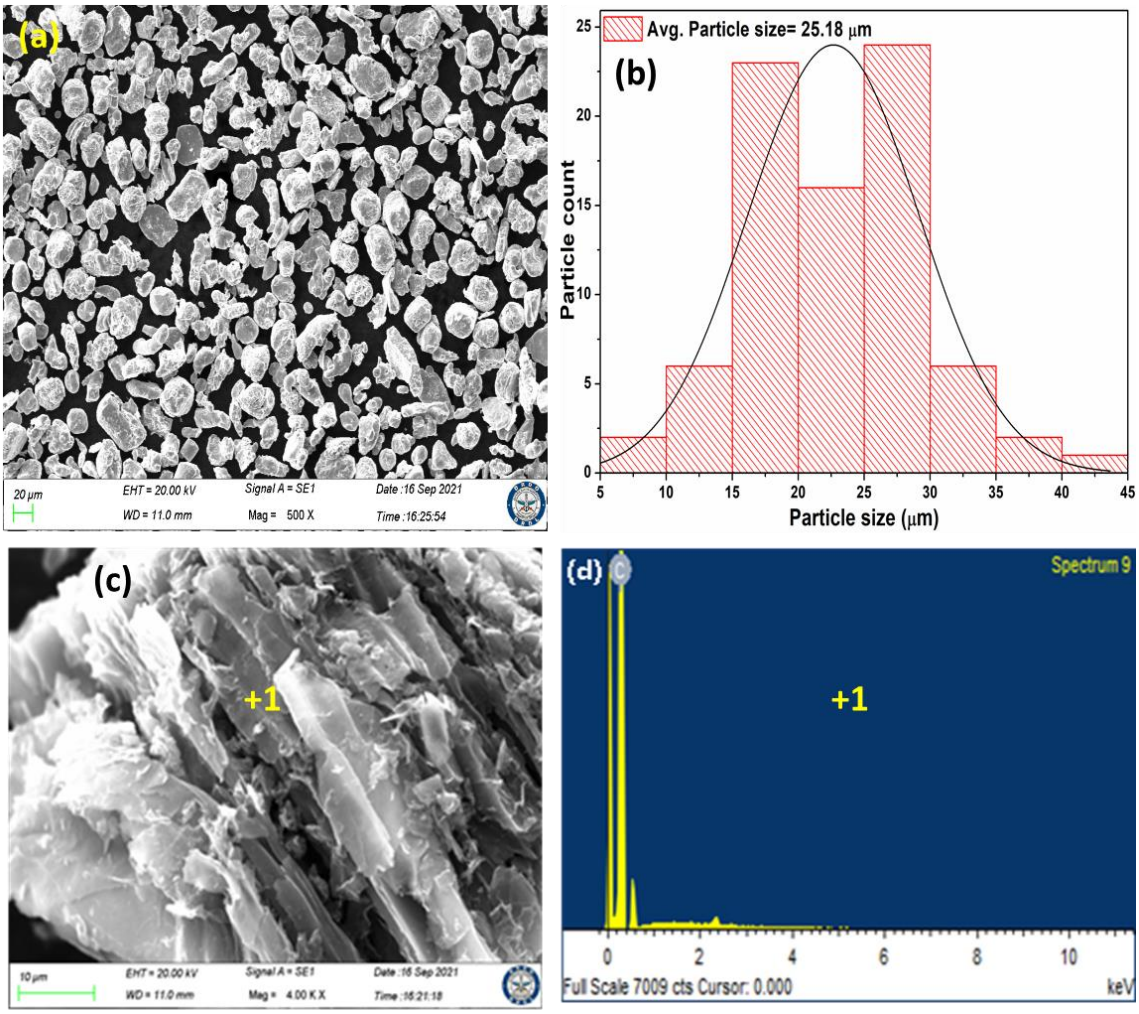

Fig. 1(a) Morphology of as-received SS316L (b) Particle size distribution of as-received SS316L (c) morphology of GNP (d) EDS map of GNP

2.2 Fabrication of composites

The GNP powder was initially mixed with ethanol for 30 minutes with a magnetic stirrer. Thereafter, the SS316L and GNP powder solutions were ultrasonicated at 10 kHz for uniform dispersion of the powders. The composite solution was placed in a hardened steel vial and mechanically alloyed for 2 hours at 300 rpm with a ball-to-powder ratio of 10:1. Then the milled composite powder was taken out of the vial and put on a hot plate to evaporate the ethanol and finally a uniformly mixed ultra-fine powder was obtained. The same processing steps were followed for other compositions. The ultra-fine composite powders were cold compacted at 600 MPa [18] to prepare test samples of the dimensions 65 mm x 15 mm x 5 mm for the tensile test. Disc samples of 20 mm in diameter and 6 mm in thickness were prepared for the SEM investigations and the hardness test. All the SS316L-GNP (0.25, 0.5, and 0.75 wt%) composite samples were isothermally consolidated at 1400^{o}C in a vacuum furnace for 90 minutes and compared with the base SS316L. The density of the sinters was measured by using the

PRE-PRINT ARTICLE
COPYRIGHT BY COMPOSITES THEORY AND PRACTICE JOURNAL
ISSN: 2299-128X

Archimedes water immersion principle. The theoretical densities of the composites were calculated utilizing the rule of mixtures formula. The relative density was evaluated by the ratio of the sintered to the theoretical density. E8 tensile test specimens were cut from the above prismatic sample using a wire-cut EDM. The following procedure was adapted to develop the composites as presented in Fig. 2.

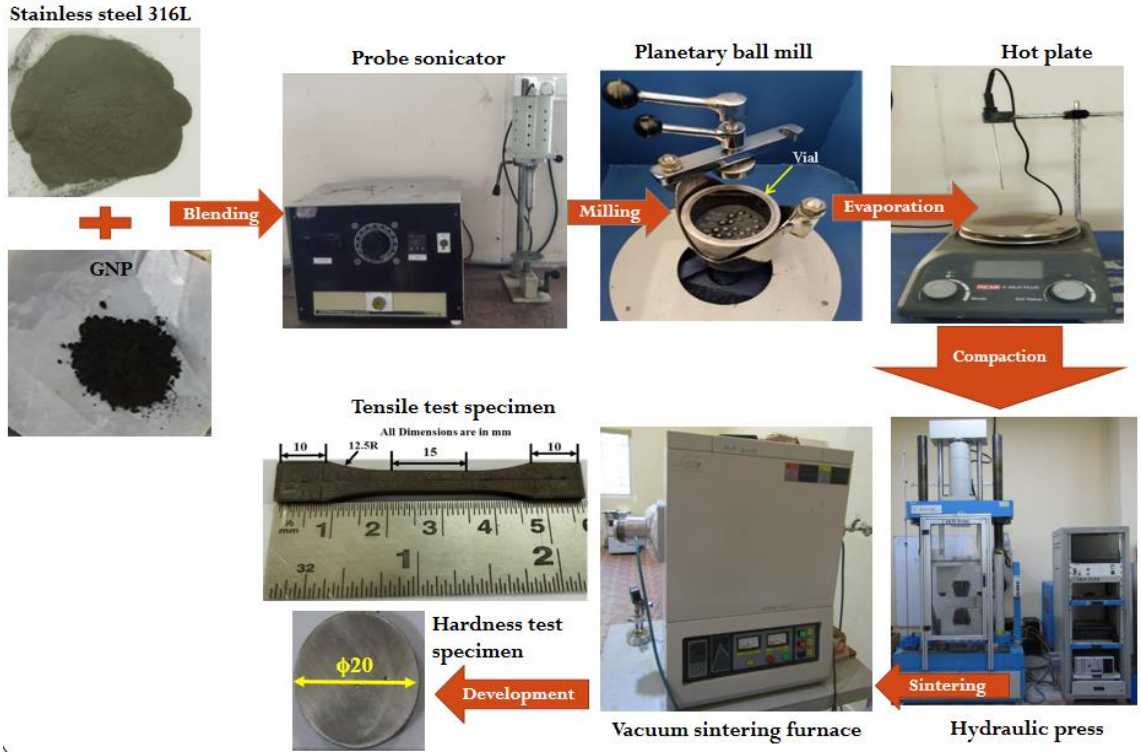

Fig. 2. Fabrication steps for development of composites

2.3 Characterization and mechanical testing

Phase quantification was done on an X-ray diffractometer (Smart Lab SE, Rigaku, Japan) with Cu-kα radiation (λ=0.154056 nm) at the scan speed of 5˚/min over the 2θ range of 20˚-80˚. The disc samples were polished with different grades of sandpaper having varying grit sizes from 180 to 4000. Fine polishing was done with alumina powder and then diamond paste was applied to obtain a scratch free surface on the samples. All the samples were dried with hot air after being cleaned with distilled water. Furthermore, the samples were etched with aqua regia reagent (75% HNO_3 and 25% HCl) for 30 s. The etched samples were examined using a light microscope (BX53M, Olympus, Japan) and a scanning electron microscope (EVO MA10, Carl Zeiss, Germany). The tensile properties of the base SS316L, SS316L- GNP (by wt% of 0.25, 0.5, and 0.75) reinforced composites were determined by means of a universal testing machine (INSTRON-1362, USA) as per ASTM-E8 standards. The Vickers hardness test was conducted utilizing a micro-Vickers hardness

PRE-PRINT ARTICLE
COPYRIGHT BY COMPOSITES THEORY AND PRACTICE JOURNAL
ISSN: 2299-128X

tester (FSA, FMV-1, India) at the load of 1 kgf for a 10 s dwell time. The average value was calculated by performing five successive indentations.

3. Results and discussion

3.1 Densification behavior

The theoretical density values for the SS316L-GNP compositions were calculated using the rule of mixtures by considering the theoretical density values of 7.87 g/cm^3 and 2.1 g/cm^3, respectively, for SS316L and GNP. Table 1 lists the relative density values of the SS316L-GNP composites contain different weight percentages of GNP. The relative densities of SS316L and SS316L with the addition of GNP were found to be 97.45, 97.54, 97.71, and 97.11%, respectively. By increasing the GNP content up to 0.5 wt%, the relative densities of the composites rose slightly. Increasing the GNP content has no significant effect on the relative density, which indicates appropriate diffusion of the layers (one upon another) and higher sintering temperatures [19]. When the powders were sintered at near or more than the melting temperature (>1400^{o}C), the liquid phase was formed. This causes capillary force, which quickly rearranges the particles by diffusion and mass transport mechanisms, leading to better densification [20,21]. However, the relative density slightly dropped for the 0.75 wt% composite sample. As revealed in the SEM studies (Fig. 5d), the composite is expected to have GNP agglomerations that decrease the densification [22]. Cao et al. obtained higher relative densities, which indicate good interfacial bonding of GNP in oxide dispersion strengthened (ODS) steels and uniform dispersion.

Table. 1 Density, microhardness, and tensile properties of SS316L and SS316-GNP (0.25, 0.5, 0.75 wt%) composites.

Sample	Sintered density (gm/cm^3)	Relative density (%)	Hardness (Hv)	Ultimate tensile strength (MPa)	Elongation (%)
SS316L[a]	8.0	--	155	515	60%
SS316L	7.6697	97.45	134.5± 5	418.6± 20.7	21.32
SS316L-0.25 wt% GNP	7.6247	97.54	270.1± 7	508.32± 18.1	18.34
SS316L-0.5 wt% GNP	7.5860	97.71	289.7± 6	554.62± 17.4	14.64
SS316L-0.75 wt% GNP	7.4887	97.11	282.6± 4	439.56± 21.4	6.53

[a]https://asm.matweb.com/search/SpecificMaterial.asp?bassnum=mq316q

PRE-PRINT ARTICLE
COPYRIGHT BY COMPOSITES THEORY AND PRACTICE JOURNAL
ISSN: 2299-128X

3.2 Phase analysis

The XRD pattern of the SS316L-xGNP(x: 0.25, 0.5, 0.75 wt%) sintered samples is shown in Fig. 3. The XRD pattern of the as-received GNP powder was also considered for comparison purposes. Only austenite phases (γ) were detected in all the samples corresponding the hkl planes of (111), (200), and (220) at 44.2°, 51.3°, and, 75.1° as is confirmed by COD card no. 9015774. Moreover, by varying the GNP content (0.25, 0.5, and 0.75 wt%) in SS316L, the austenite phase was not altered. In the SS316L-0.75 wt% composites, the chromium carbide phase (Cr_7C_3) phase was detected with JCPDS card no. 00-036-1482 at 1400°C [23]. The reason was that the Cr atoms in the matrix diffused with the carbon atoms in GNP to form chromium carbides [24]. In our study, we observed that the formation of carbides at 0.75 wt% GNP contributed to improvement in the yield strength and hardness. Nevertheless, these carbides might introduce challenges such as increased brittleness or reduced ductility. This causes early failure of the components depending on the amount of carbides present in the sample [25, 26]. No oxide peaks were observed in the diffraction pattern, which means that oxidation was restricted because the sintering experiments were conducted in vacuum.

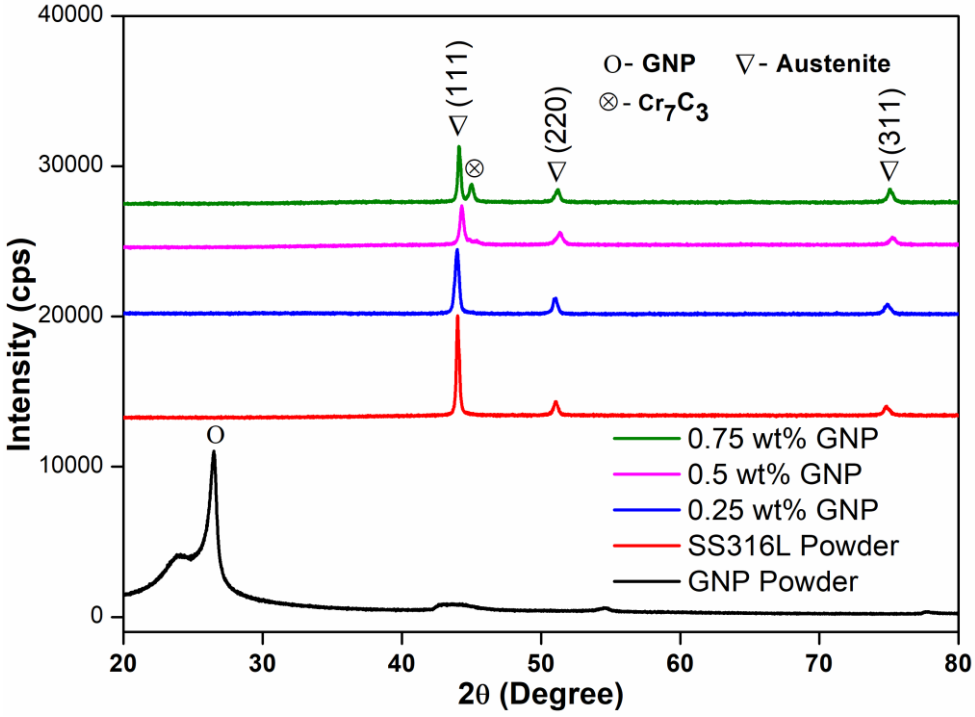

Fig. 3. XRD spectrum of SS316L-GNP composites (by wt%)

3.3 Microstructure observations

Fig. 4(a-d) shows the microstructure of the SS316L and SS316L-GNP composites with different wt% GNP sintered at 1400°C for 90 min. The black color distribution indicates etching pits, and GNP are located along the grain boundaries. The base 316L steel sample has a typical equiaxed and twin-grain

PRE-PRINT ARTICLE
COPYRIGHT BY COMPOSITES THEORY AND PRACTICE JOURNAL
ISSN: 2299-128X

structure [27, 28]. The average grain size of austenite of 31.06 μm was measured from Fig. 4 (a) using ImageJ software. The 316L-0.25 and 0.5 wt% GNP composites presented in Fig. 4 (b) and (c), clearly demonstrate the better dispersion of GNP in the steel matrix along the grain boundaries [17]. The reason is that at the liquid phase sintering temperature of 1400°C, the viscosity of the liquid is significantly reduced due to capillary action, which enables good wetting characteristics between the austenite and GNP. The austenite grain size was reduced to 25.65 μm and 23.06 μm for the 316L-0.25 and 0.5 wt% GNP composites, respectively, which follow the Hall-Petch relationship [29]. The microstructure of the SS316L-0.75 wt% GNP composite in Fig. 4(d) shows a coarse grain structure of 143.74 μm. Severe melt pool distribution was observed due to high sintering temperatures [30]. Upon heating at liquidus temperatures (≥1400ºC), liquid melt pools form from the austenite that occupies the surrounding grain boundaries [31]. Moreover, Cr-carbides formed along the grain boundaries. This causes grain coarsening, which further deteriorates the mechanical properties of the composites. Typically, the presence of carbides and melt pools at the grain boundaries can be associated with localized grain coarsening by influencing the mobility of grain boundaries and the kinetics of grain growth [32].

3.4 Composite morphology

To better comprehend the surface morphology of the composites, SEM observation was carried out in different regions of the composite. Fig. 5(a) shows the SEM micrograph of the base SS316L, which reveals twin austenite and pores. Fig. 5(b and c) shows the GNP distribution along the grain boundaries. After introducing GNP to SS316L at 0.25 and 0.5 wt%, a reduction in the pore size was observed. Furthermore, GNP anchored between the grain boundaries inhibits grain growth of the matrix, which produces a fine grain structure [17, 33]. Also, at the liquid phase sintering temperature of 1400°C, the viscosity of the liquid is significantly reduced as a consequence of capillary action, which facilitates good wetting between the austenite and GNP. This is an important insight as it suggests that the liquid phase plays a crucial role in the wetting and interaction between the matrix (austenite) and the graphene nanoplatelets. On the other hand, the SEM micrograph in Fig. 5(d) of the 0.75 wt% GNP reinforced composite reveals a coarse grain structure owing to the formation of carbides (Cr_7C_3), which were detected by XRD studies [26]. As the sintering temperature grows, the carbon in GNP diffuses with the matrix to fully or partially form carbides. Nonetheless, when comes cooling, this Cr and C resolidify and form stable Cr carbides. This was shown by the widened light grey intermediate region as shown in Fig. 5(d). Also, the EDS results showed the weight and atomic fractions of Cr and C of 17.85 and 14.19 and 34.32 and 11.81, respectively, confirming the presence of Cr_7C_3 carbides. In addition, it was proved thermodynamically by substituting temperature (T) in

PRE-PRINT ARTICLE
COPYRIGHT BY COMPOSITES THEORY AND PRACTICE JOURNAL
ISSN: 2299-128X

the Gibbs energy of formation (ΔG_f^o) in the following equation. The standard Gibbs energy of formation for Cr_7C_3 is about -151 kJ/mol. The results are consistent with previous works [34, 35].

$$\Delta G_f^o(Cr7C3) = -92067 - 41.5\,T\ J/mol$$

Moreover, agglomeration was found when GNP were added in higher wt%, which deteriorates the mechanical properties as explained in previous studies. Saboori et al. reported that significant improvement was achieved in the mechanical properties of Al/GNP composites due to grain refinement. In addition to that, GNP agglomeration was evident by increasing the wt% of GNP [22].

3.5 Elemental composition

Fig. 6 displays the EDS measurements of the SS316L and SS316L-GNP (0.25, 0.5, 0.75 wt%) composites. Table 2 presents the elemental composition of the SS316L and SS316L-GNP composites. Carbon was not detected due to the low amount and the remaining elements of Fe, Cr, Mo, and Si were detected in the base SS316L. After performing EDS at intergranular sites for the 0.25 wt% and 0.5 wt% GNP composites, it was found that the carbon signal was higher. Furthermore, the Fe and Ni contents decreased in the intergranular region of the SS316L-0.75 wt% GNP composite. The SS316L-0.75 wt% GNP had higher chromium and carbon signals at the grain boundaries compared to base SS316L, which indicates that the grain boundary contains chromium-rich carbide.

PRE-PRINT ARTICLE

COPYRIGHT BY COMPOSITES THEORY AND PRACTICE JOURNAL

ISSN: 2299-128X

Polish Society of Composite Materials

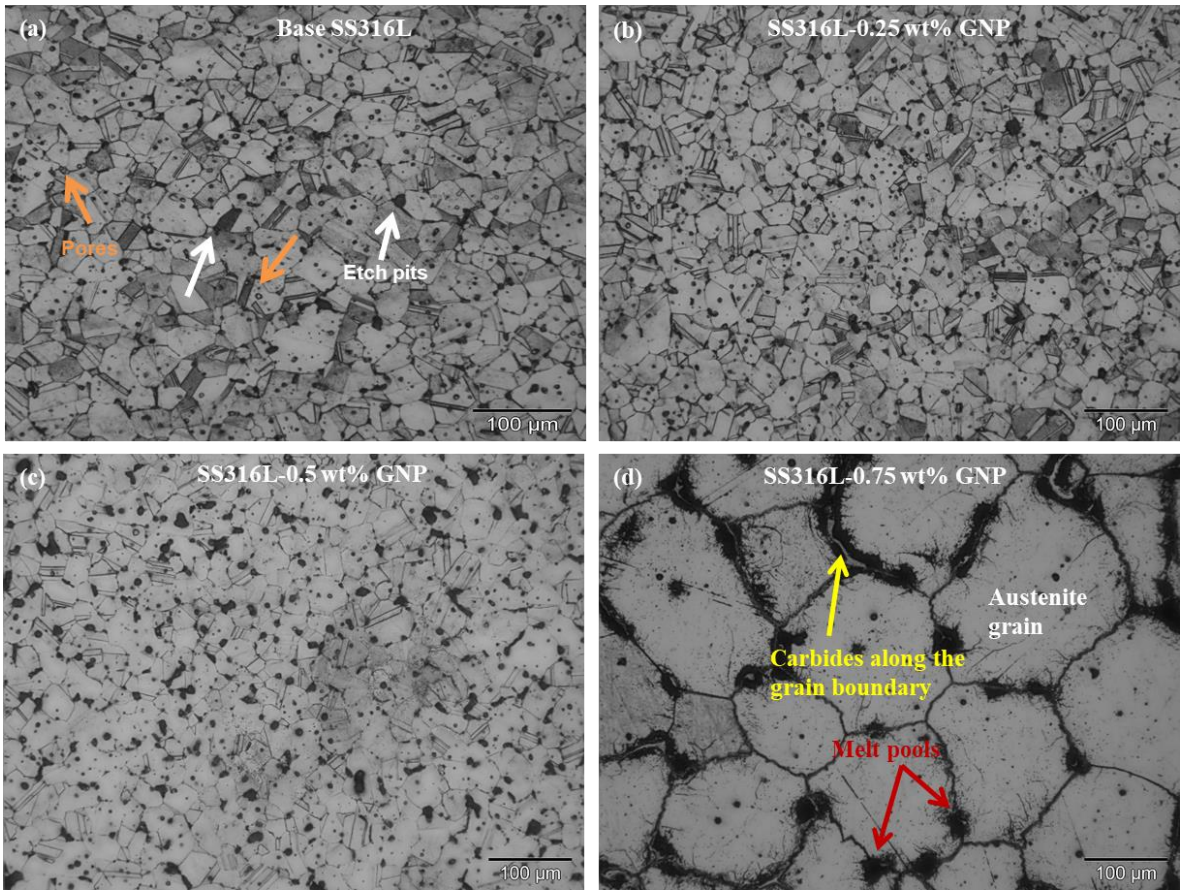

Fig. 4. Microstructure of (a) base SS316L (b-d) GNP composites (0.25, 0.5, and 0.75 wt%)

PRE-PRINT ARTICLE

COPYRIGHT BY COMPOSITES THEORY AND PRACTICE JOURNAL

ISSN: 2299-128X

Polish Society of Composite Materials

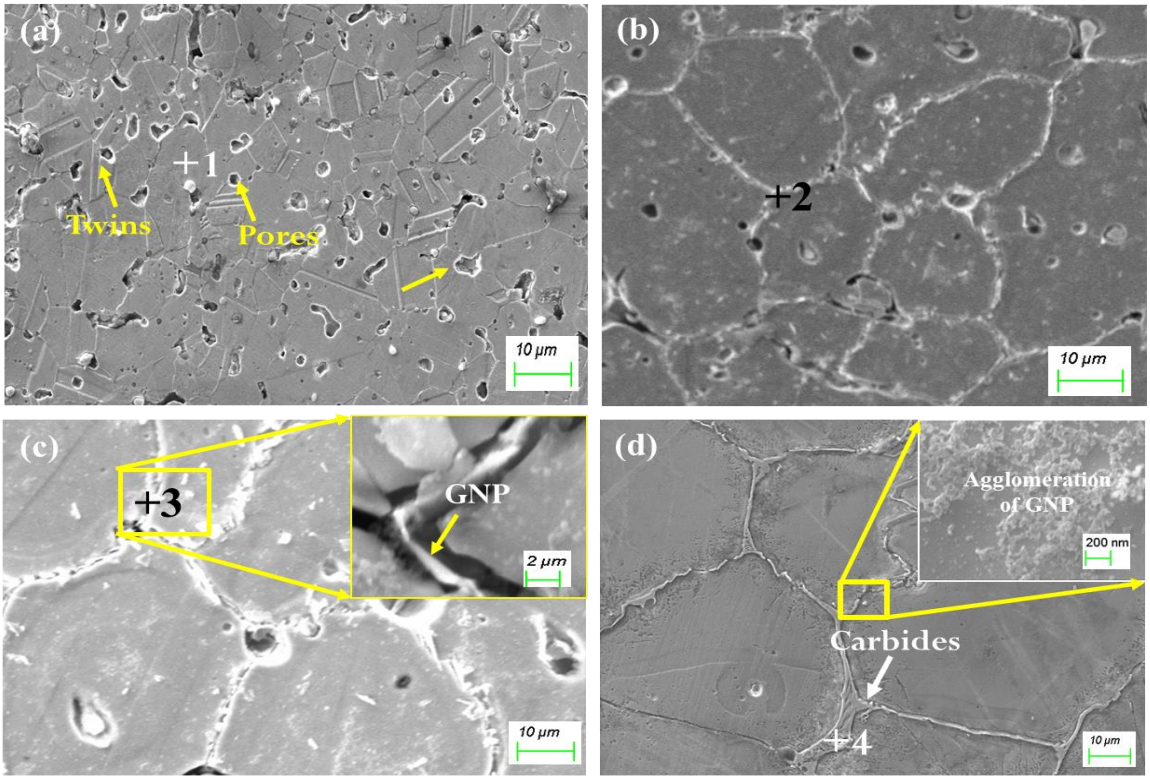

Fig. 5. SEM micrographs of (a) SS316L (b) SS316L-0.25 wt% GNP (c) SS316L-0.5 wt% GNP (d) SS316L-0.75 wt% GNP composites

PRE-PRINT ARTICLE
COPYRIGHT BY COMPOSITES THEORY AND PRACTICE JOURNAL
ISSN: 2299-128X

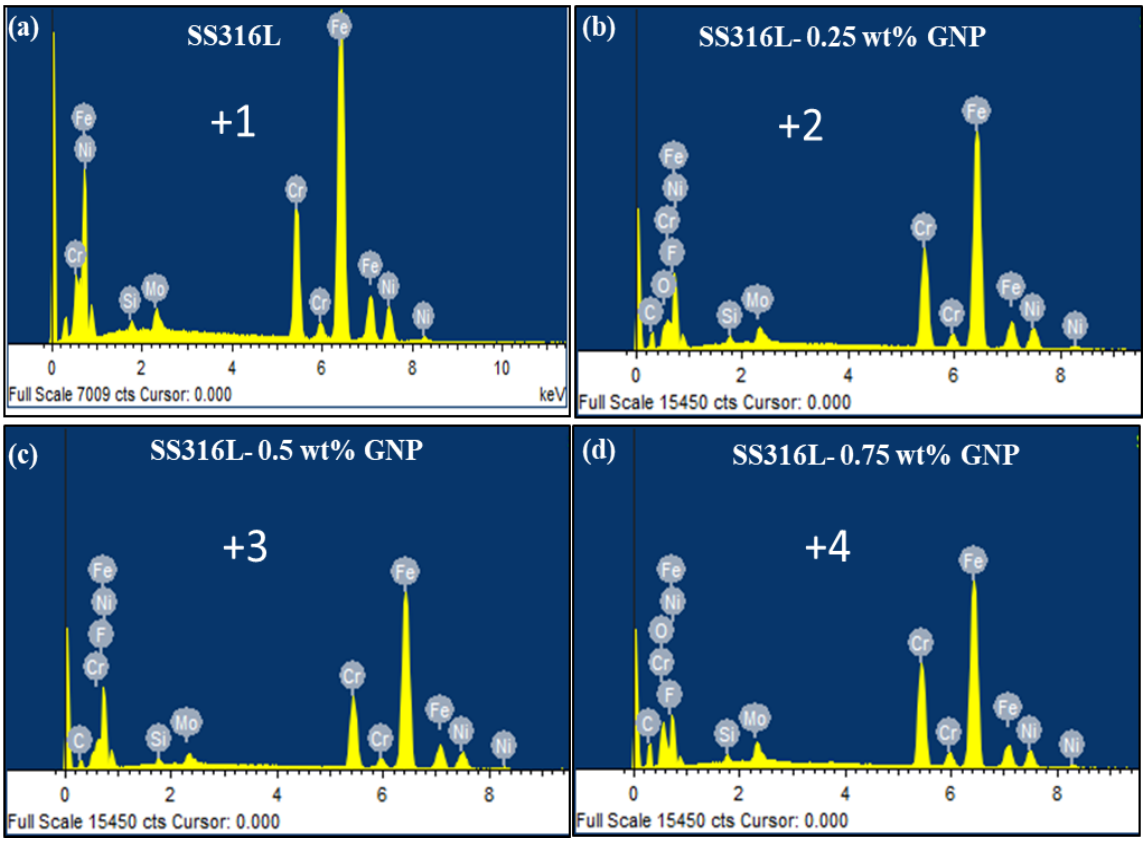

Fig. 6. EDS compositional analysis of SS316L and SS316L-GNP composites

Table 2. Elemental composition of SS316L and SS316L-GNP composites

Sample	Elements (wt%)					
	FeK	CrK	NiK	MoL	CK	SiK
Base SS316L	69.11	16.35	10.80	3.17	-	0.57
SS316L-0.25 wt% GNP	62.49	16.41	9.83	2.89	7.82	0.56
SS316L-0.5 wt% GNP	61.09	16.48	9.23	2.48	10.16	0.56
SS316L-0.75 wt% GNP	56.68	17.85	8.28	2.46	14.19	0.54

3.6 Ultimate tensile strength

Fig. 7 (a) shows the stress-strain curves for the different SS316L-GNP composites processed at 1400ºC for the sintering time of 90 min. The variations in the ultimate tensile strength (UTS) and elongation are given in Table 1. As observed from the graph, the UTS of the unreinforced SS316L is 418.6 MPa. However, the strength value grew by 21.4% with the addition of 0.25 wt% GNP to the SS316L matrix material. A further increase in GNP content from 0.25 to 0.5 wt% raised the strength value to 32.5%. The SS316L-0.5 wt% GNP composite attained the highest tensile strength value of 554.62 MPa. The notable change in the strength values might be due to the presence of GNP, grain boundary strengthening, an increase in dislocation density, and effective load transfer from the matrix to the reinforcement [26,29,36]. Nonetheless, with a further increase in the fraction of GNP from 0.5 to

PRE-PRINT ARTICLE
COPYRIGHT BY COMPOSITES THEORY AND PRACTICE JOURNAL
ISSN: 2299-128X

0.75, the strength of the SS316L composite dropped. This is because of uneven grain distribution and grain coarsening, resulting in weak bonding between the steel matrix and GNP reinforcement [37]. Furthermore, the formation of agglomerated zones (Fig. 5(d)), which weakens the 316L/GNP interface, is also a factor for poor strength. On the other hand, the elongation percentage was significantly decreased by increasing the graphene weight percentage. The percentage elongation values of SS316L, and SS316L-xGNP(x: 0.25, 0.5, and 0.75 wt%) are 60, 21.32, 18.34, 14.64 and 6.53%, respectively. The GNP were pinned at the grain boundaries, leading to grain refinement, which in turn led to low ductility. This causes a notable increment in the ultimate tensile strength and hardness. The SS316L-0.75 wt% composite fractures at low elongation compared to others owing to the brittleness of the chromium carbide phase. These conclusions are similar to those made by researchers for different materials [38-40].

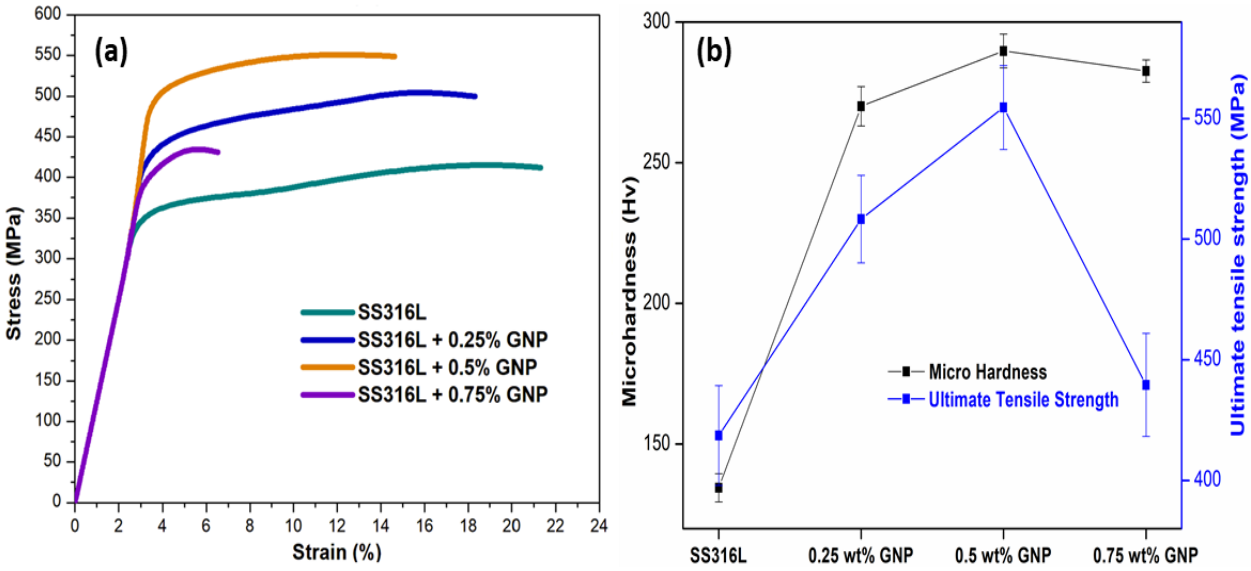

Fig. 7 (a) stress vs strain plot (b) variation in Vickers microhardness and ultimate tensile strength of SS316L-GNP composites

3.7 Vickers hardness

The microhardness of 316L stainless steel consolidated at 1400°C is 134.5 Hv. The hardness grew to 270.1 Hv with the addition of 0.25 wt% GNP at the same sintering temperature. As seen in Fig. 7(b), the hardness was substantially enhanced with the addition of 0.5 wt% GNP to SS316L. The nanocomposite with 0.5 wt% GNP reinforcement exhibited a greater hardness of 289.7 Hv than all the other composites. The increase in the weight fraction of GNP reinforcement enables hardness improvement [41]. Because the GNP were located at the grain boundaries, they hinder grain growth, which in turn produces a refined grain structure as explained in the light microscopy studies. Another reason is that there is a large thermal mismatch between the GNP and SS316L matrix, which is also likely to increase hardness. A decrease in hardness was observed at 0.75 wt% GNP in SS316L [28].

PRE-PRINT ARTICLE
COPYRIGHT BY COMPOSITES THEORY AND PRACTICE JOURNAL
ISSN: 2299-128X

This results from agglomeration taking place with the higher GNP content, which weakens the reinforcement/SS316L matrix interface [42]. Shashanka et al. reported that low porosity and higher shrinkage at 1400°C were responsible for the improvement in hardness and density owing to an increase in mass transport that created necking and improved bonding between the powder particles [43].

Conclusions

SS316L composites with different wt% of GNP were successfully fabricated by pressureless sintering at the liquidus temperature of 1400°C for 90 minutes. Some of the key findings are summarized below:

- Only the austenitic phase was observed in the XRD spectrum of all the composites. The GNP phase was not detected by the XRD because the GNP content is low. The Cr-carbide phase was detected only in the composite with 0.75 wt% GNP.

- The 0.5 wt% GNP composite achieved the highest density due to the capillary action of a liquid phase that fills pores located near the grain boundaries. Beyond 0.5 wt% GNP, the relative density of composites fell as a consequence of GNP agglomeration.
- GNP was effective in refining the grain size. The composite with 0.5 wt% GNP exhibited a smaller grain size (23.06 μm) compared to the base SS316L (31.06 μm).
- The 0.75 wt% GNP composite revealed the presence of carbides and melt pools at intergranular sites.
- From the EDS studies, it was found that the rising trend of Cr and C content resulted in the formation of carbides at the grain boundaries.
- The 0.5 wt% GNP reinforced stainless steel 316L exhibited a 32.5% improvement in the ultimate tensile strength
- The hardness doubled in the 0.5 wt% GNP composite compared to the base SS316L.

These findings suggest that the addition of GNP has a significant impact on the microstructure and mechanical properties of SS316L. The 0.5 wt% GNP composite appears to be particularly promising, showing improved density, grain refinement, and enhanced mechanical properties. This study also highlights challenges associated with higher GNP concentrations, such as a reduced relative density due to agglomeration and the formation of carbides.

REFERENCES

(1) sintered powder metallurgy 316L stainless steel," *Mater. Des.*, vol. 52, pp. 995–998, 2013, doi: 10.1016/j.matdes.2013.06.035.
(2) S. S. Panda, V. Singh, A. Upadhyaya, and D. Agrawal, "Effect of conventional and microwave sintering on the properties of yttria alumina garnet-dispersed austenitic stainless steel," *Metall. Mater. Trans. A Phys. Metall. Mater. Sci.*, vol. 37, no. 7, pp. 2253–2264, 2006,

doi: 10.1007/BF02586144.

(3) H. S. Kim, "Densification mechanisms during hot isostatic pressing of stainless steel powder compacts," *J. Mater. Process. Technol.*, vol. 123, no. 2, pp. 319–322, 2002, doi: 10.1016/S0924-0136(02)00104-8.

(4) S. Pandya, K. S. Ramakrishna, A. Raja Annamalai, and A. Upadhyaya, "Effect of sintering temperature on the mechanical and electrochemical properties of austenitic stainless steel," *Mater. Sci. Eng. A*, vol. 556, pp. 271–277, Oct. 2012, doi: 10.1016/j.msea.2012.06.087.

(5) M. Wang, H. Sun, L. Zou, G. Zhang, S. Li, and Z. Zhou, "Structural evolution of oxide dispersion strengthened austenitic powders during mechanical alloying and subsequent consolidation," *Powder Technol.*, vol. 272, pp. 309–315, 2015, doi: 10.1016/j.powtec.2014.12.008.

(6) A. Raja Annamalai, A. Upadhyaya, and D. K. Agrawal, "Effect of heating mode and Y2O3 addition on electrochemical response on austenitic and ferritic stainless steels," *Corros. Eng. Sci. Technol.*, vol. 50, no. 2, pp. 91–102, 2015, doi: 10.1179/1743278214Y.0000000176.

(7) P. K. Kumar, N. V. Sai, and A. G. Krishna, "Effect of Y2O3 addition and cooling rate on mechanical properties of Fe-24Cr-20Ni-2Mn steels by powder metallurgy route," *Compos. Commun.*, vol. 10, pp. 116–121, 2018, doi: 10.1016/j.coco.2018.09.003.

(8) D. Kim, H. Kang, D. Bae, S. Nam, M. Quevedo-Lopez, and H. Choi, "Synthesis of reduced graphene oxide/aluminum nanocomposites via chemical-mechanical processes," *J. Compos. Mater.*, vol. 52, no. 22, pp. 3015–3025, 2018, doi: 10.1177/0021998318760152.

(9) V. Khanna, V. Kumar, and S. A. Bansal, "Mechanical properties of aluminium-graphene/carbon nanotubes (CNTs) metal matrix composites: Advancement, opportunities and perspective," *Mater. Res. Bull.*, vol. 138, no. December 2020, p. 111224, 2021, doi: 10.1016/j.materresbull.2021.111224.

(10) M. Khoshghadam-Pireyousefan, R. Rahmanifard, L. Orovcik, P. Švec, and V. Klemm, "Application of a novel method for fabrication of graphene reinforced aluminum matrix nanocomposites: Synthesis, microstructure, and mechanical properties," *Mater. Sci. Eng. A*, vol. 772, p. 138820, 2020, doi: 10.1016/j.msea.2019.138820.

(11) S. Chatterjee, F. A. Nüesch, and B. T. T. Chu, "Comparing carbon nanotubes and graphene nanoplatelets as reinforcements in polyamide 12 composites," *Nanotechnology*, vol. 22, no. 27, 2011, doi: 10.1088/0957-4484/22/27/275714.

(12) W. Zhou, Y. Fan, X. Feng, K. Kikuchi, N. Nomura, and A. Kawasaki, "Creation of individual few-layer graphene incorporated in an aluminum matrix," *Compos. Part A Appl. Sci. Manuf.*, vol. 112, pp. 168–177, 2018, doi: 10.1016/j.compositesa.2018.06.008.

(13) S. Ali, A. M. A. Rani, K. Altaf, and Z. Baig, "Investigation of Boron addition and compaction pressure on the compactibility, densification and microhardness of 316L Stainless Steel," *IOP Conf. Ser. Mater. Sci. Eng.*, vol. 344, no. 1, 2018, doi: 10.1088/1757-899X/344/1/012023.

(14) A. Sadooghi and G. Payganeh, "Effects of sintering process on wear and mechanical behavior properties of titanium carbide/hexagonal boron nitrid/steel 316L base nanocomposites," *Mater. Res. Express*, vol. 5, no. 2, 2018, doi: 10.1088/2053-1591/aaaf7a.

(15) S. S. Kumar, E. S. Sandeep, S. B. Chandrasekhar, and S. K. Karak, "Development of nano-oxide dispersed 304L steels by mechanical milling and conventional sintering," *Mater. Res.*, vol. 19, no. 1, pp. 175–182, 2016, doi: 10.1590/1980-5373-MR-2015-0593.

(16) E. Zengin, H. Ahlatci, and H. Zengin, "Investigation of microstructure, tribological and corrosion properties of AISI 316 L stainless steel matrix composites reinforced by carbon nanotubes," *Mater. Today Commun.*, vol. 29, no. May, p. 102758, 2021, doi: 10.1016/j.mtcomm.2021.102758.

(17) A. V. Radhamani, H. C. Lau, M. Kamaraj, and S. Ramakrishna, "Structural, mechanical and tribological investigations of CNT-316 stainless steel nanocomposites processed via spark plasma sintering," *Tribol. Int.*, vol. 152, no. July, p. 106524, 2020, doi: 10.1016/j.triboint.2020.106524.

(18) S. R. Kandala, K. Balani, and A. Upadhyaya, "Mechanical and electrochemical characterization of supersolidus sintered austenitic stainless steel (316 L)," *High Temp. Mater. Process.*, vol. 38, no. 2019, pp. 792–805, 2019, doi: 10.1515/htmp-2019-0032.

(19) A. Mandal *et al.*, "Tribological behavior of graphene-reinforced 316L stainless-steel composite prepared via selective laser melting," *Tribol. Int.*, vol. 151, no. May, p. 106525, 2020, doi: 10.1016/j.triboint.2020.106525.

(20) R. M. German, P. Suri, and S. J. Park, "Review: Liquid phase sintering," *J. Mater. Sci.*, vol. 44, no. 1, pp. 1–39, 2009, doi: 10.1007/s10853-008-3008-0.

(21) R. Bollina, S. J. Park, and R. M. German, "Master sintering curve concepts applied to full-density supersolidus liquid phase sintering of 316L stainless steel powder," *Powder Metall.*, vol. 53, no. 1, pp. 20–26, 2010, doi: 10.1179/174329009X409688.

(22) A. Saboori, S. K. Moheimani, M. Dadkhah, M. Pavese, C. Badini, and P. Fino, "An overview of key challenges in the fabrication of metal matrix nanocomposites reinforced by graphene nanoplatelets," *Metals (Basel).*, vol. 8, no. 3, 2018, doi: 10.3390/met8030172.

(23) K. Hirota, K. Mitani, M. Yoshinaka, and O. Yamaguchi, "Simultaneous synthesis and consolidation of chromium carbides (Cr3C2, Cr7C3 and Cr23C6) by pulsed electric-current pressure sintering," *Mater. Sci. Eng. A*, vol. 399, no. 1–2, pp. 154–160, 2005, doi: 10.1016/j.msea.2005.02.062.

(24) F. Martín, C. García, Y. Blanco, and M. L. Rodriguez-Mendez, "Influence of sinter-cooling rate on the mechanical properties of powder metallurgy austenitic, ferritic, and duplex stainless steels sintered in vacuum," *Mater. Sci. Eng. A*, vol. 642, pp. 360–365, 2015, doi: 10.1016/j.msea.2015.06.097.

(25) C. Boonruang and W. Sanumang, "Effect of nano-grain carbide formation on electrochemical behavior of 316L stainless steel," *Sci. Rep.*, vol. 11, no. 1, pp. 1–11, 2021, doi: 10.1038/s41598-021-91958-x.

(26) W. Ren *et al.*, "A Facile and Cost-Effective Approach to Fabricate In-Situ Synthesized Graphene Nanosheet Reinforced 316L Stainless Steel," *Jom*, vol. 72, no. 12, pp. 4514–4521, 2020, doi: 10.1007/s11837-020-04440-w.

(27) G. A. Rao and M. Kumar, "High performance stainless steel via powder metallurgy hot isostatic pressing," *Mater. Sci. Technol.*, vol. 13, no. 12, pp. 1027–1032, 1997, doi: 10.1179/mst.1997.13.12.1027.

(28) V. Kalyanamanohar and A. Gopalakrishna, "Effect of SiC coated GNP on microstructure and mechanical properties of pressureless sintered SS316L composites," *i-manager's J. Mech. Eng.*, vol. 12, no. 3, p. 1, 2022, doi: 10.26634/jme.12.3.18589.

(29) A. Mandal, J. K. Tiwari, N. Sathish, and A. K. Srivastava, "Microstructural and mechanical properties evaluation of graphene reinforced stainless steel composite produced via selective laser melting," *Mater. Sci. Eng. A*, vol. 774, no. January, p. 138936, 2020, doi: 10.1016/j.msea.2020.138936.

(30) X. Yang, F. Gao, F. Tang, X. Hao, and Z. Li, "Effect of Surface Oxides on the Melting and Solidification of 316L Stainless Steel Powder for Additive Manufacturing," *Metall. Mater. Trans. A Phys. Metall. Mater. Sci.*, vol. 52, no. 10, pp. 4518–4532, 2021, doi: 10.1007/s11661-021-06405-3.

(31) A. Sharon and D. Itzhak, "Mechanical properties of sintered austenitic stainless steel-effect of silicon addition," *Mater. Sci. Eng. A*, vol. 157, no. 2, pp. 145–149, 1992, doi: 10.1016/0921-5093(92)90021-R.

(32) E. Gamsjäger, D. M. Ogris, and J. Svoboda, "Kinetics of grain boundary networks controlled by triple junction and grain boundary mobility," *Metals (Basel).*, vol. 8, no. 12, 2018, doi: 10.3390/met8120977.

(33) W. Ouyang *et al.*, "Multilayer-graphene reinforced 316L matrix composites preparation by laser deposited additive manufacturing: Microstructure and mechanical property analysis," *Mater. Res. Express*, vol. 6, no. 9, Jul. 2019, doi: 10.1088/2053-1591/ab2f2e.

[34] L. Fu *et al.*, "Microstructure and tribological properties of Cr3C2/Ni3Al composite materials prepared by hot isostatic pressing (HIP)," *Mater. Des.*, vol. 115, no. February, pp. 203–212, 2017, doi: 10.1016/j.matdes.2016.11.060.

(35) M. Small and E. Ryba, "CALCULATION AND EVALUATION OF THE GIBBS ENERGIES OF FORMATION OF Cr3C2, Cr7C3, and Cr23C6.," *Metall. Trans. A, Phys. Metall. Mater. Sci.*, vol. 12 A, no. 8, pp. 11389–11396, 1981, doi: 10.1007/bf02643683.

(36) S. Wen, K. Chen, W. Li, Y. Zhou, Q. Wei, and Y. Shi, "Selective laser melting of reduced graphene oxide/S136 metal matrix composites with tailored microstructures and mechanical properties," *Mater. Des.*, vol. 175, p. 107811, 2019, doi: 10.1016/j.matdes.2019.107811.

(37) G. Jeong *et al.*, "The effect of grain size on the mechanical properties of aluminum," *Arch. Metall. Mater.*, vol. 60, no. 2, pp. 1287–1291, 2015, doi: 10.1515/amm-2015-0115.

(38) M. D. Umar, R. Muraliraja, V. S. Shaisundaram, and S. G. Wayessa, "Influence of Future Material Nano-ZrO2and Graphene on the Mechanical Properties of Al Composites," *J. Nanomater.*, vol. 2022, 2022, doi: 10.1155/2022/1454037.

(39) S. Yang *et al.*, "Effects of the graphene content on mechanical properties and corrosion resistance of aluminum matrix composite," *J. Mater. Res. Technol.*, vol. 28, no. September 2023, pp. 1900–1906, 2024, doi: 10.1016/j.jmrt.2023.12.059.

(40) W. S. AbuShanab, E. B. Moustafa, E. Ghandourah, and M. A. Taha, "Effect of graphene nanoparticles on the physical and mechanical properties of the Al2024-graphene nanocomposites fabricated by powder metallurgy," *Results Phys.*, vol. 19, no. August, 2020, doi: 10.1016/j.rinp.2020.103343.

(41) M. Rashad, F. Pan, A. Tang, and M. Asif, "Effect of Graphene Nanoplatelets addition on mechanical properties of pure aluminum using a semi-powder method," *Prog. Nat. Sci. Mater. Int.*, vol. 24, no. 2, pp. 101–108, 2014, doi: 10.1016/j.pnsc.2014.03.012.

(42) V. Subbaiah, B. Palampalle, and K. Brahmaraju, "Microstructural Analysis and Mechanical Properties of Pure Al–GNPs Composites by Stir Casting Method," *J. Inst. Eng. Ser. C*, vol. 100, no. 3, pp. 493–500, 2019, doi: 10.1007/s40032-018-0491-1.

(43) R. Shashanka and D. Chaira, "Development of nano-structured duplex and ferritic stainless steels by pulverisette planetary milling followed by pressureless sintering," *Mater. Charact.*, vol. 99, pp. 220–229, 2015, doi: 10.1016/j.matchar.2014.11.030.